ANALYSIS OF COLD-FORMED OPEN STEEL SECTIONS UNDER SIMPLE BENDING

Nadia S. N. Ota
Eduardo M. Batista
nadia.ota@coc.ufrj.br
batista@coc.ufrj.br
Programa de Engenharia Civil – COPPE – UFRJ
Centro de Tecnologia – Av. Horácio Macedo, s/n – Cidade Universitária, 21941-450, Rio de Janeiro, Brasil
Juarez M. S. Franco
juarezfranco@ufrrj.br
Instituto de Tecnologia, Universidade Federal Rural do Rio de Janeiro
Rodovia Br 465, km 07, s/n – Zona Rural, Seropédica –RJ, Brasil

Abstract. Cold-formed open steel sections under flexural loading are subjected to the combined phenomena of bending, local (L), distortional (D), global (G) buckling and flange curling. Some of the main challenges in evaluating the results obtained by numerical and experimental analysis are (i) defining the displacement portion due to each one of these phenomena, as some of them occur in the same plane of loading; (ii) the presence of intermediate stiffeners in these members makes the buckling modes classification imprecise. Additionally, it is known that small changes in the section geometry may imply large variations in the structural performance. This paper analyzes stiffened CFS beams through Finite Strip Method (elastic stability analysis) and Finite Element Method (non-linear analysis with arc-length control for strength prediction). The careful records of the displacements by numerical analysis, combined with linear regression techniques, allowed evaluating the evolution of the different mechanical phenomena during loading. The contribution of the stiffener height variation on the critical bending moments was investigated. Particular interest is addressed to the strength erosion due to the modal LD interaction, since the tendency of $M_{crL}/M_{crD} = 1$ ratio is obtained by optimization methods where the objective function is directed towards the maximization of critical moments. In this work, the geometric parameters were defined in order to generate variations of the commercial self-supporting roofing tile RT-260/620 (Regional Telhas), with steel plate thickness of 0.95 mm.

Keywords: Cold-formed open steel sections, Buckling modes interaction, Initial imperfection, Flange curling.

1   Introduction

Cold-formed open steel sections (CFS) are widely used in light construction, due to their low self-weight, which makes their transport, storage, handling and installation easier, faster and more economical and their high strength/weight ratio, displaying the efficient use of the material. This efficiency can be enhanced through an appropriate choice of the cross-section configuration, in which the intermediate stiffeners play an important role. The CFS manufacturing process allows a versatility of cross-section shapes; however, their mechanical performance is heavily dependent on small changes in their configuration. The development of free softwares, as CUFSM [1], based on the Finite Strip Method, or GBTul [2] based on the Generalized Beam Theory, for the design and analysis of CFS, stimulated the use and study of these elements in civil construction.

CFS walls present a high width/thickness ratio, leading to a complex stability behavior in elastic buckling, developing local (L), distortional (D) and global (G) modes and affecting the element strength, as these instability phenomena commonly occur before the yielding of the section. In the local buckling mode, the cross-section walls buckle without any movement of their junctions. In the distortional buckling mode, the junctions move together with the walls, causing a distortion to the cross-section. When the local and distortional critical loadings present similar values, it may occur a local-distortional (LD) interaction, affecting the section strength. The interaction between the buckling modes has been studied by researchers as Dinis et al. [3] Dinis and Camotim [4], Matsubara et al. [5].

Self-supporting roofing tiles of cold-formed steel sections are used to cover great spans due to its lightness. The strength of these sections is heavily influenced by their shape. Self-supporting roofing tiles usually present a trapezoidal shape, with two oblique webs, a bottom flange and two top flanges on each side. In order to increase the strength of these sections, some intermediate stiffeners with various geometric configuration are added, which help to prevent the local buckling of the elements. The position, type and size of the intermediate stiffeners in the compressed walls have a great influence on the dominant buckling mode. These intermediate stiffeners are generally trapezoidal, "V" and "Z" shaped, and placed in the webs and/or in the flanges. The enhancement in strength depends on the type, number, position and dimension of the stiffener.

The influence of intermediate stiffeners on profiled steel decks was studied by Bernard et al. [6], [7], who performed an experimental analysis of the buckling modes of these tiles under bending load. They analyzed flat-hat and V-stiffeners with varying height, positioned on the compressed flange and proposed a design method for profiled steel decks with intermediate stiffeners [8].

The flange curling in profiled steel decks were also studied by Bernard et al. [9]. Flange curling is the tendency of the flanges, the most stressed regions, of a thin walled section to move towards the neutral axis when subject to bending as the curvature increases. The wider the flange, the more prominent is the phenomenon. Flange curling does not depend on the span length, but rather on the thickness and width of flange. Winter [10] was the first to propose an equation to the flange curling that relate these variables.

Franco et al. [11] proposed Shape Grammar rules for cold-formed steel profiles. Manufacturing limitations and defined stiffeners sizes were prescribed by the Shape Grammar, resulting in manufacturable cross-sections. Melo et al. [12] identified the most appropriate configuration of intermediate stiffeners for self-supporting roofing tiles. Franco and Batista [13] combined Shape Grammar and Finite Strip analysis for determining the geometric parameters that most influence the buckling behavior in stiffened trapezoidal profiled sheeting. Garcia et al. [14] reviewed the criteria for modal identification in stiffened trapezoidal steel sections and presented a numerical analysis that indicates the local-distortional buckling modes interaction in these elements.

The technical literature on the behavior of stiffened trapezoidal steel sections is in a development phase, in this sense, there are few theoretical studies on this theme with numerical and experimental validation, aiming, among others objectives, improvements in the normative procedures. Self-supporting roofing tiles present a great number of geometric variables, with intermediate stiffeners of different types and dimensions, leading to a complex analysis and design. The offer of these roofing tiles is restricted to the catalogs of the manufacturers. The study of these sections allows improvements in these products.

The objective of the present work is to develop a numerical analysis on the structural behavior of cold-formed self-supporting steel sections with intermediate stiffeners under bending loading, addressed to large span roofing systems, analyzing the displacements under the local and distortional buckling modes, and their interaction, as well as, the displacements due to bending and flange curling, in order to be able to separate the influence of each of these phenomena on the buckling mode and strength.

The numerical model in shell finite elements was developed using the commercial software ANSYS. This numerical model enabled the analysis of the commercial roofing profile RT-260/620 (Regional Telhas).

2   Self-supporting roofing tile RT-260/620

The commercial (Regional Telhas) self-supporting roofing tile RT-260/620 is a trapezoidal tile with a trapezoidal stiffener in its bottom flange and a rounded and two Z stiffeners on each web. Figure 1 presents its dimensions. These tiles are rolled cold-formed and are sold in 0.8, 0.95, 1.25 and 1.55 mm thickness.
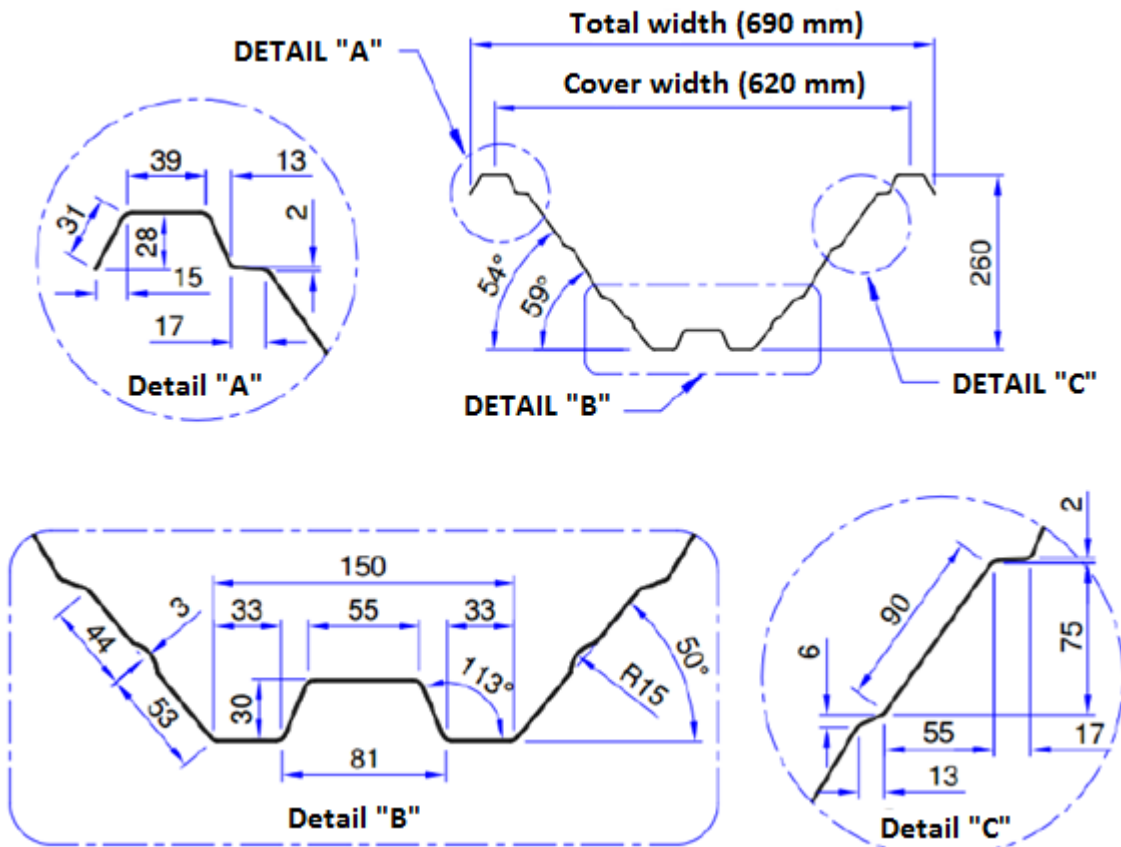
Figure 1: Self-supporting roofing tile RT-260/620 by Regional Telhas. Source: Regional Telhas Technical Information sheet.

3   Influence of the height of the trapezoidal stiffener

Considering the roofing tile RT-260/620 with thickness of 0.95 mm, linear elastic material (steel) with Young's modulus of 200 000 N/mm2 and Poisson's ratio of 0.3, simply supported under pure bending loading of 1kNm, the bottom flange in compression due to the wind suction loads, the buckling critical moments were computed using the CUFSM software for a range of wavelengths.

The analysis was performed varying the height of the trapezoidal stiffener of the compressed flange (Figure 2). The width of 81 mm of the stiffener base and the 113° angle of its walls were kept

constant. The height h of the stiffener varied from 0 to 40 mm, in 1 mm steps. As the stiffener height increased, the length of its top reduced proportionally, from 81 mm for 0 mm height, to 46.4 mm for 40 mm height.

h = 0 mm   h = 5 mm   h = 10 mm

h = 20 mm   h = 30 mm   h = 40 mm
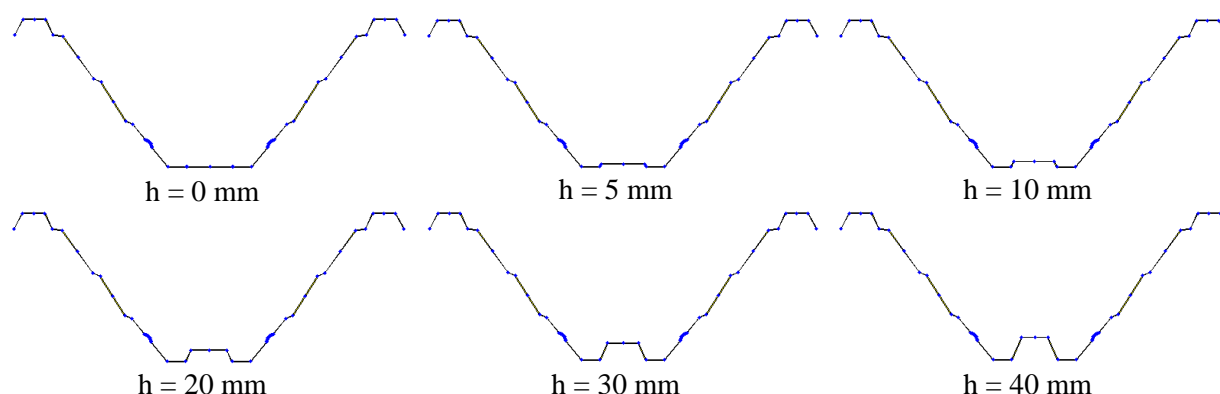
Figure 2: Trapezoidal stiffener height variation.

The roofing tile presents four buckling modes: (i) symmetric local; (ii) asymmetric distortional; (iii) symmetric distortional and (iv) asymmetric distortional 2 (Figure 3).

a) Symmetric local   b) Asymmetric distortional

c) Symmetric distortional   d) Asymmetric distortional 2
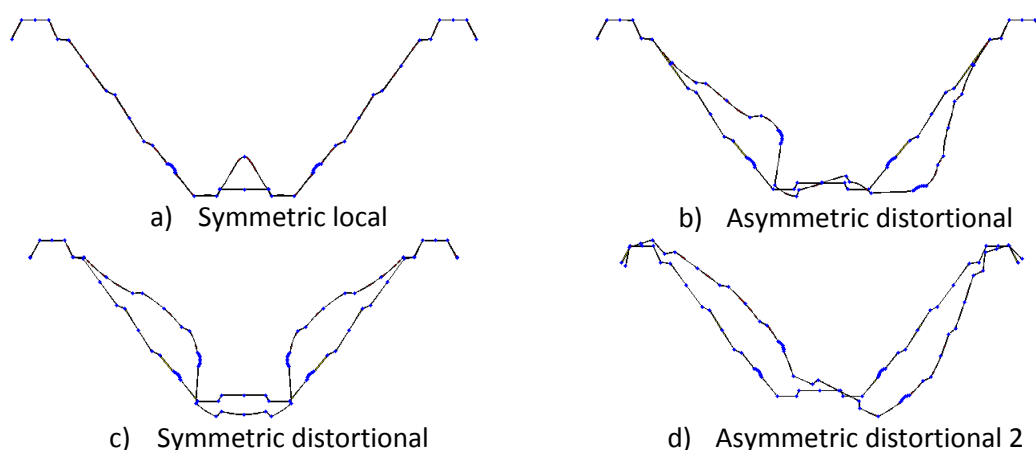
Figure 3: Buckling modes (trapezoidal stiffener with 10 mm height).

Figure 4 presents the critical moment to the trapezoidal stiffener height graph. The critical moment of the symmetric local mode varied from 9.27 kNm (for h = 2 mm) to 31,4 kNm (for h = 40 mm). This critical moment increases with the increase of the stiffener height because the top width of the stiffener decreases, decreasing its slenderness. The asymmetric distortional mode presents a subtle reduction in the critical moments values, from 17 kNm (h = 6 mm) to 16 kNm (h = 40 mm). The values of the critical moment of the symmetric distortional mode increased from 2.6 kNm (to h = 0 mm) to 18 kNm (for h= 10 mm); no critical moments values were presented till h = 34 mm where it increased again from 52 kNm (h = 34 mm) to 53 kNm (h = 40 mm). As for the asymmetric distortional 2 mode, the critical moment values changed from 28.7 kNm (for h = 0mm) to 45 kNm (for h = 40mm).

For trapezoidal stiffener heights too low (0, 1 and 2 mm) prevails the symmetric distortional mode. Between h = 3 mm and h = 17 mm, the symmetric local mode prevails. From 18 mm above, the asymmetric distortional mode presents the lowest critical moment. As the height of the stiffener increases, this critical moment slightly decreases, in a way that increasing the stiffener height does not influence the dominant buckling mode and its critical moment value.
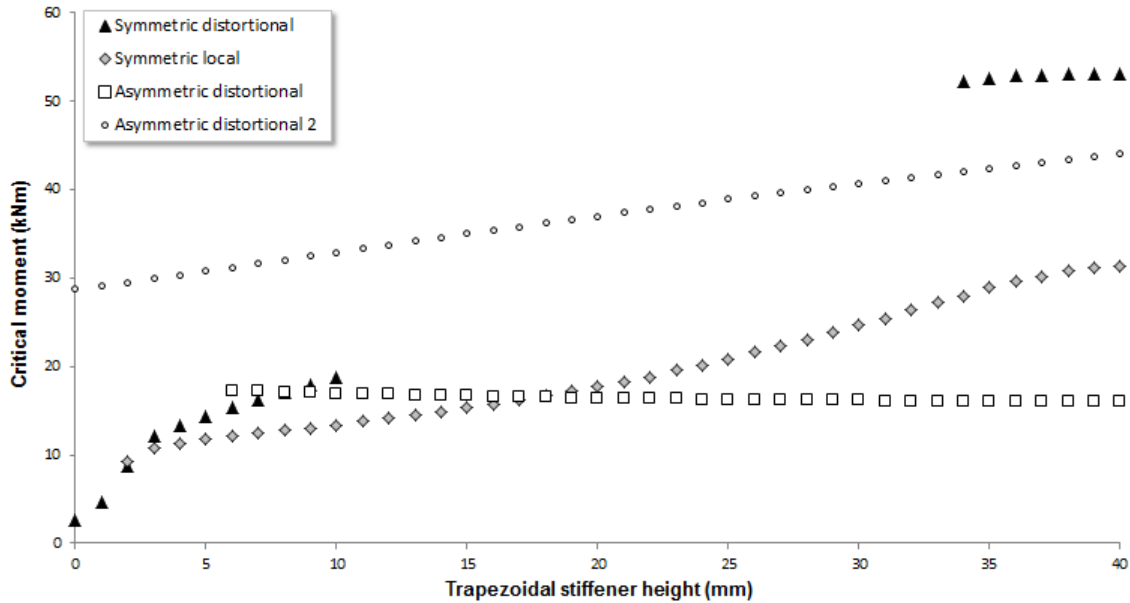
Figure 4: Influence of the trapezoidal stiffener height.

4 R2 coefficient analysis

The coefficient of determination, R^2 or R-Squared, is a statistical measure of fit that represents the proportion of the variance in the dependent variable that is predictable from the independent variable or variables in a regression model.

R^2 values range from 0 to 1 and are calculated by

$$R^2 \equiv 1 - \frac{SS_{res}}{SS_{tot}}$$

where SS_{res} is the residual sum of squares and SS_{tot} is the total sum of squares (proportional to the variance of the data).

The higher the R^2 value, closer to 1, the better the fit. An R^2 of 1 indicates that the regression predictions perfectly fit the data.

To a set of data points of displacements values along the length of a beam subject to bending, the line of best fit from a parabolic regression model represents its elastic line. As the buckling occurs, the farther the displacements points will be from the elastic line. The R^2 coefficient measures this variance and is used to determine the critical buckling moment.

As the R^2 coefficient is proportional to the wavelength, the difference in the R^2 values for local modes will be not so pronounced as the difference in the R^2 values for distortional modes.

Analyzing the R^2 values for specific points of the beam cross-section, it is possible to determine its buckling mode.

The RT-260/620 roofing tile was numerically analyzed considering 9 points along a 2000 mm length, placed at intervals of 250 mm. The thickness of 0.95 mm of the roofing tile was kept constant in all analysis and the height of the trapezoidal stiffener changed in order to attain different buckling modes (see Figure 4).

The vertical displacements (UY) of 9 points of the bottom flange were recorded in a nonlinear load time history analysis. These points were labeled as in Figure 5. Point 5C stands in the middle of the trapezoidal stiffener, and points 2L and 2R, in the middle of the left (L) or right (R) bottom flange. Points 1, 3 and 4 are corner points.
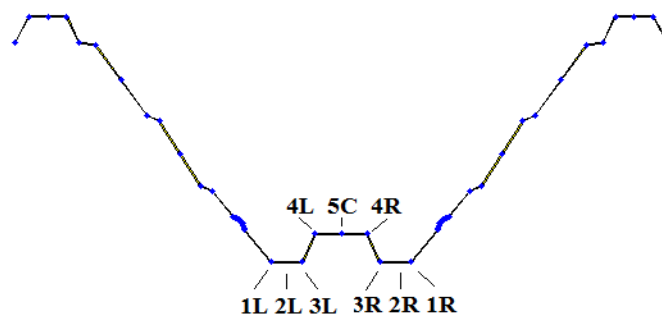
Figure 5: Label of the bottom flange points.

For a trapezoidal stiffener height of 1 mm, the R^2 vs. Moment graph (Figure 6) displays the symmetric distortional buckling mode (Figure 4) of the beam. The symmetry can be visualized as the points 1L, 2L, 3L and 4L change the R^2 value at the same amount of its symmetric points (1R, 2R, 3R and 4R, respectively). This distortional symmetric mode is characterized by the nodal points 1L and 1R, which remain in place during buckling and a crescent R^2 difference as we approach the center of the bottom flange. The buckling critical moment is 4.1 kNm. At 3.7 kNm the trapezoidal stiffener starts to buckle, leading to the symmetric distortional buckling as the height of the stiffener is too small for it to act as an efficient stiffener.
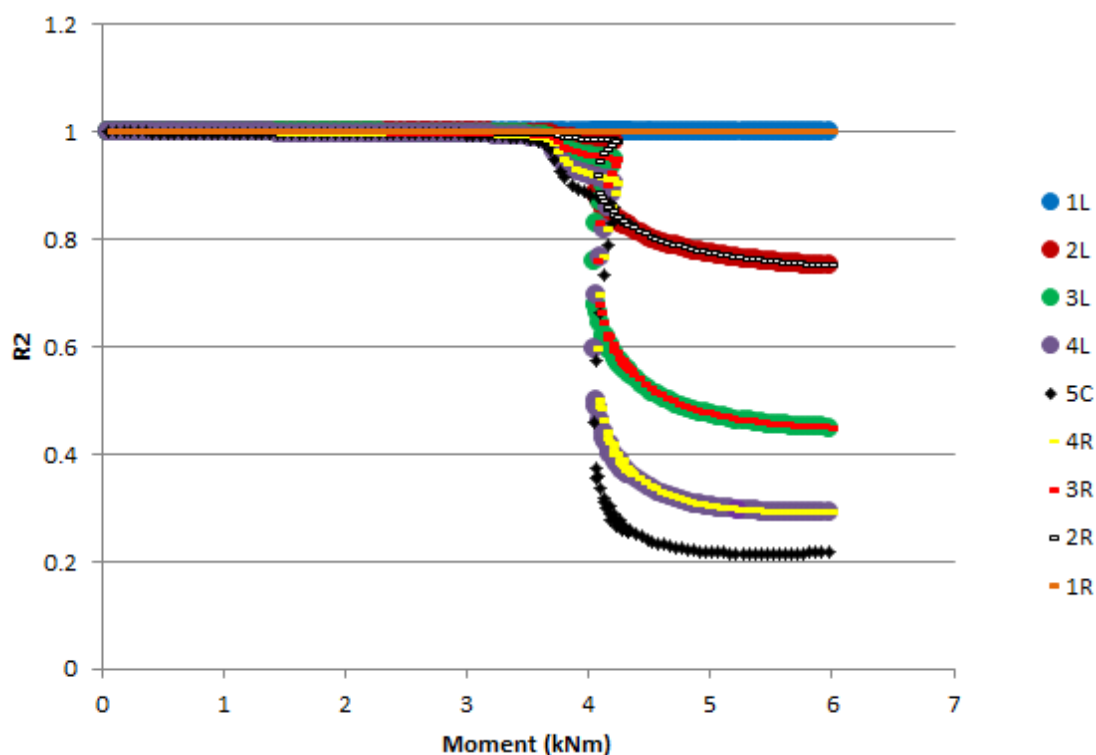
Figure 6: R2 x Moment, trapezoidal stiffener height of 1 mm.

Figure 7 presents the Moment vs. Curvature graph for the trapezoidal stiffener height of 1 mm. "k(M/EI)" is the theoretical curvature. When the beam buckles, the loss of bending stiffness can be seen by the difference in slope for the points 1L (or 1R) before and after the buckling. The point 5C shows that the buckling displacements are opposite to the bending displacements, reducing the expected beam curvature.
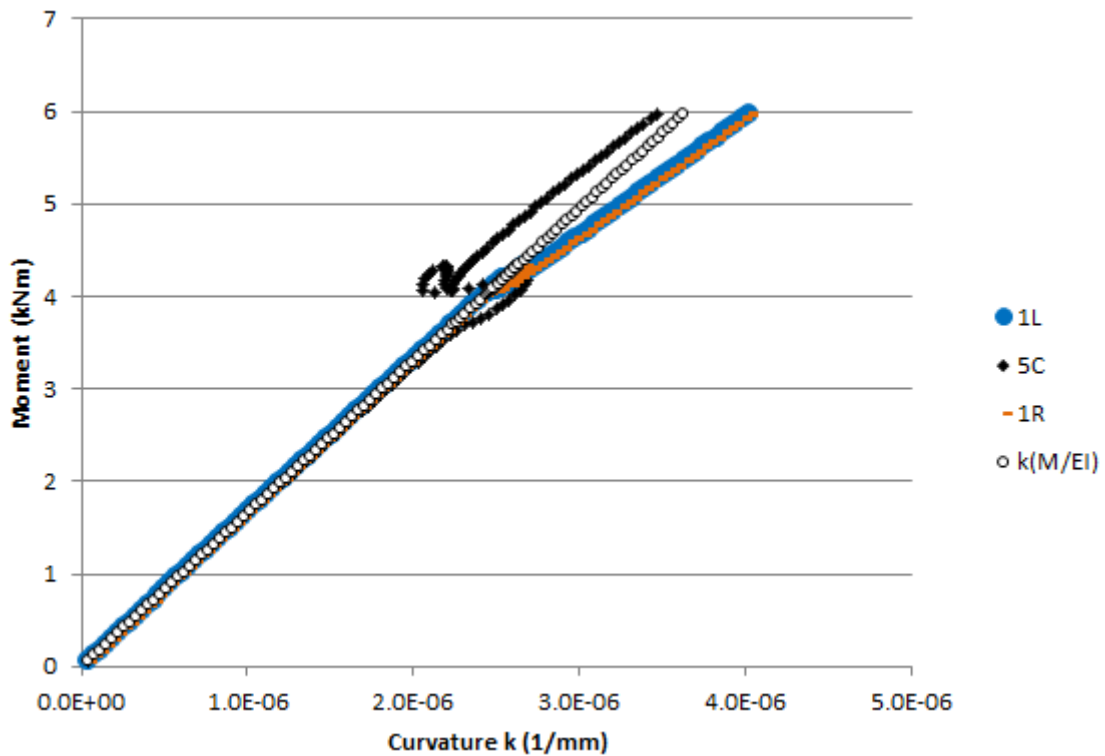
Figure 7: Moment x curvature, trapezoidal stiffener height of 1 mm.

For a trapezoidal stiffener height of 10 mm, the local buckling mode expected (Figure 3c and Figure 4) can be visualized in the R^2 vs. Moment graph (Figure 8) by the difference between the R^2 values of points 5C and 4(L or R), with a critical moment of 13 kNm. Apart from the local mode, this graph presents a symmetric distortional mode with 15 kNm critical moment. This mode interaction occurs due to the length of the beam (2000 mm), much higher than the semi-wavelength of the local and distortional critical moment (52 mm and 410 mm, respectively).

The Moment vs. Curvature graph (Figure 9) clearly exhibits the flange curling phenomenon: point 5C, which is farther from the web than point 1L or 1R, presents higher curvature than point 1 due to the addition of the flange curling displacements to the bending displacements. The local buckling mode leads point 5C to increase its curvature after buckling more than point 1.
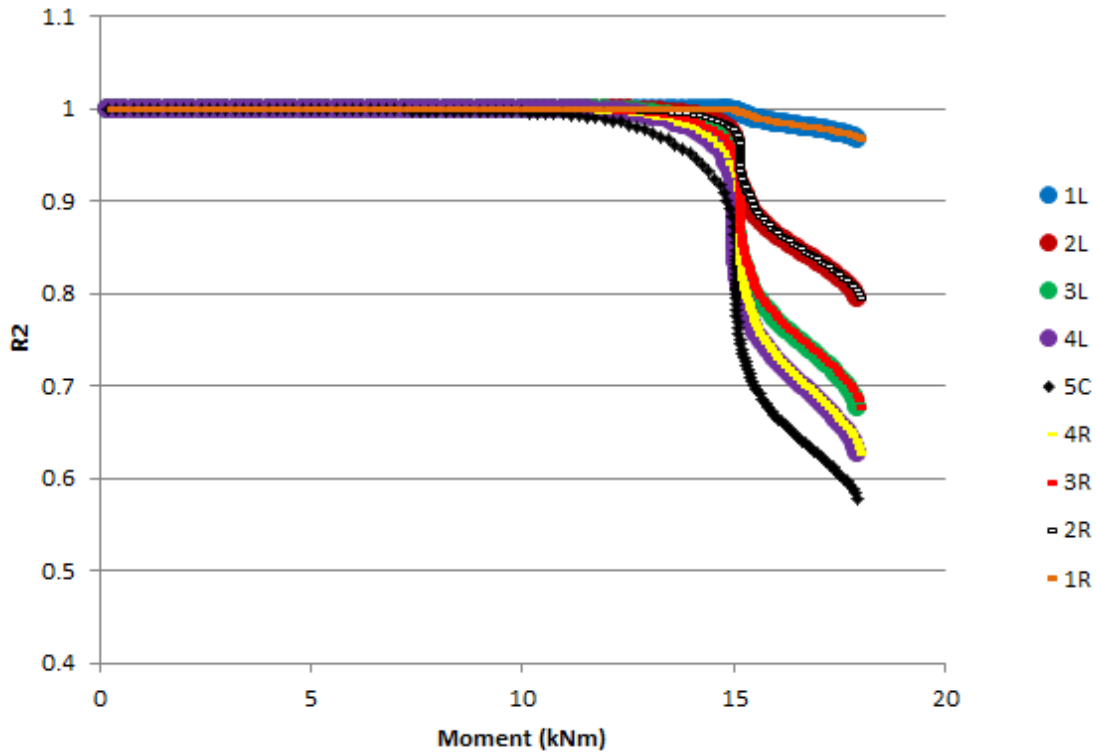
Figure 8: R2 x Moment, trapezoidal stiffener height of 10 mm.
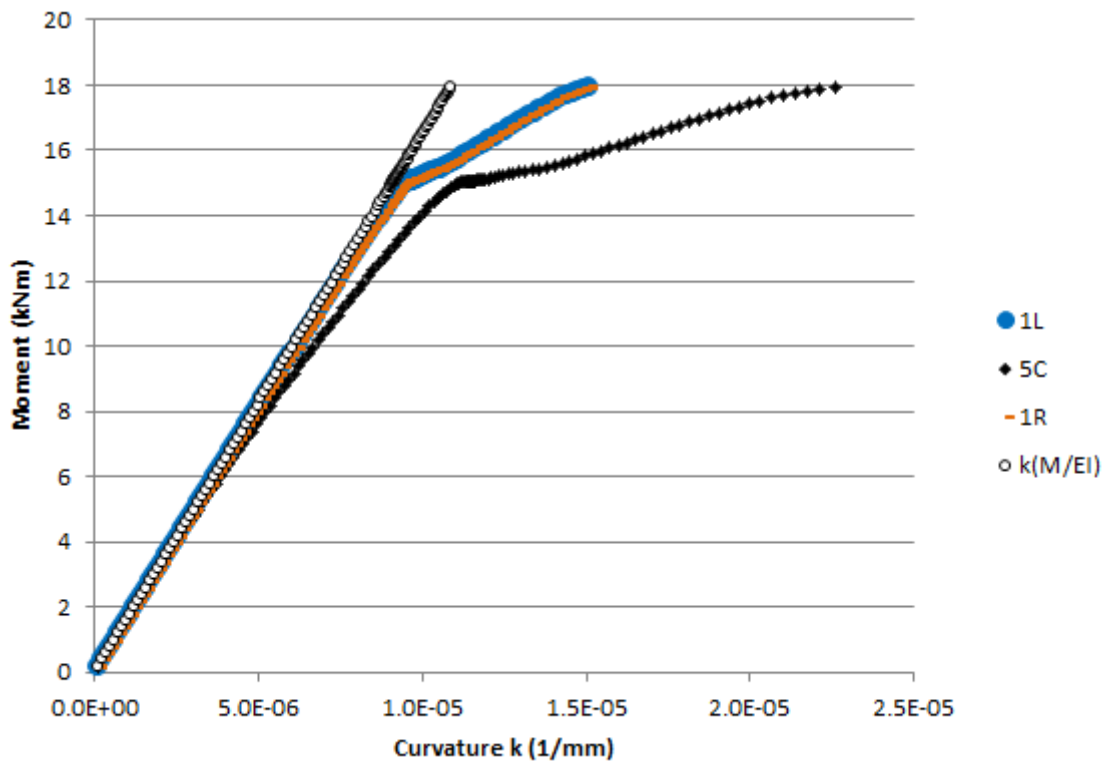
Figure 9: Moment x curvature, trapezoidal stiffener height of 10 mm.

A stiffener's height of 30 mm, leads to an asymmetric distortional mode (Figure 3b). In the R^2 vs. Moment graph, the corresponding symmetric points (L and R of points 1, 2, 3 and 4) do not present the same R^2 values (Figure 10). No local buckling at the trapezoidal stiffener is registered, as the 5C point does not change its R^2 value. The critical buckling mode is 15 kNm.
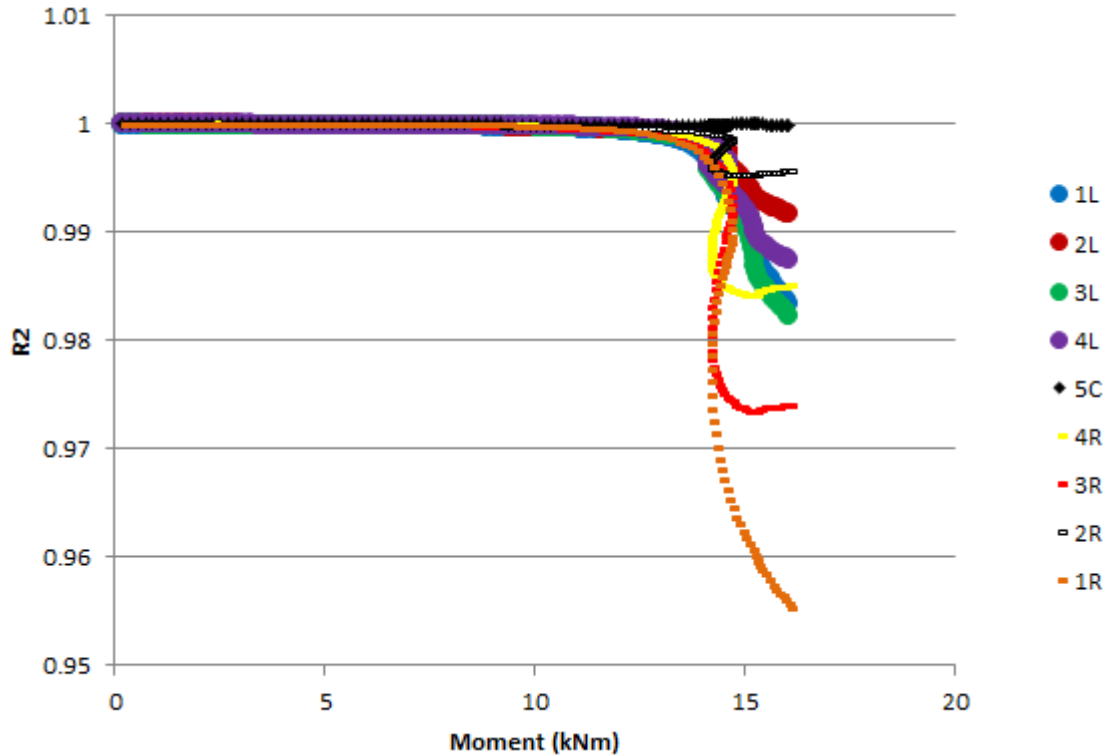
Figure 10: R2 x Moment, trapezoidal stiffener height of 30 mm, distortional initial imperfection.

The asymmetric distortional mode is presented in the Moment vs. Curvature graph (Figure 11) by the difference in curvature for points 1L and 1R after buckling. The curvature deviation of points 1L and 1R before buckling from the theoretical curvature comes from the initial imperfection adopted that affect these points.
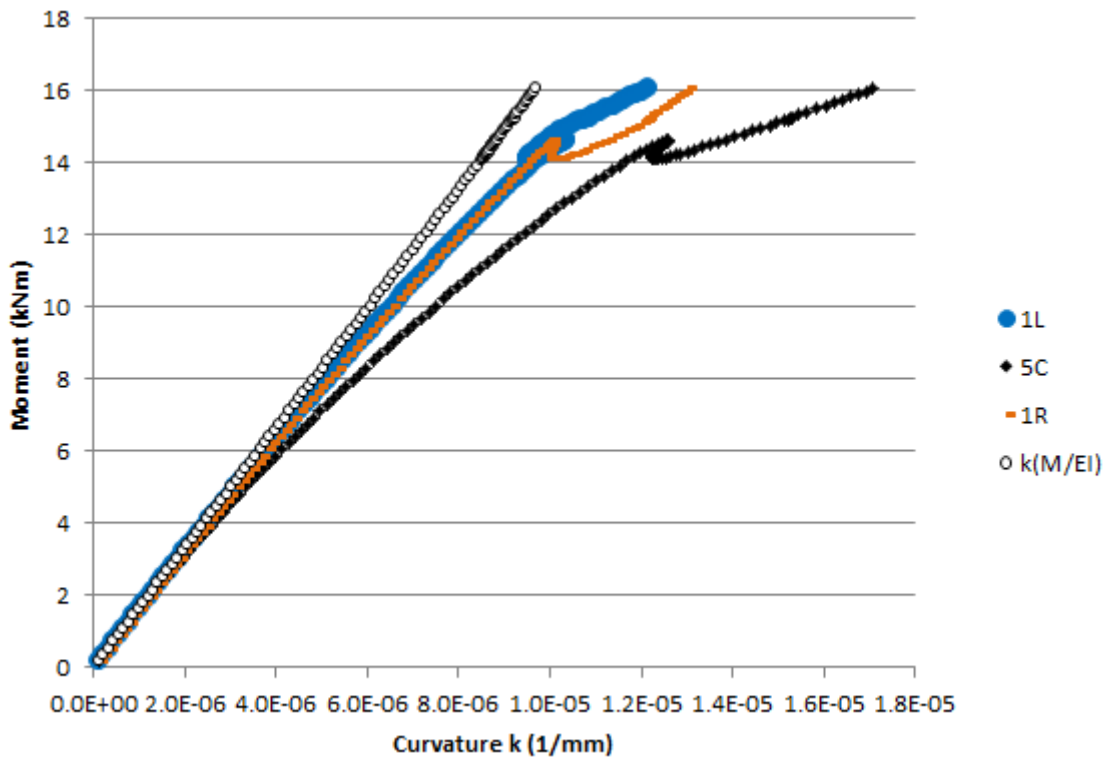
Figure 11: Moment x curvature, trapezoidal stiffener height of 30 mm, distortional initial imperfection.

4.1 The influence of the initial imperfections

The initial imperfections set for the nonlinear analysis influence the buckling mode. In this work, the geometry of the finite element model was updated to a deformed configuration by adding the displacements from a previous modal analysis by a factor of 10% of the thickness of the beam.

For the roofing tile RT-260/620, when the initial imperfections applied to the finite element model correspond to an asymmetric distortional buckling mode, it buckles in this mode, as expected. When the initial imperfections correspond to a local buckling mode of the trapezoidal stiffener, it presents an interaction of a local and a symmetric distortional buckling mode.

The symmetric distortional buckling mode is not expected in a Finite Strip analysis for the analyzed roofing tile, as it presents critical moment values too high comparing to the others buckling modes.

Figures Figure 12 and Figure 13 represent the exact same beam as the one from Figure 10 and Figure 11, differing only in the initial imperfection applied to the model: in Figure 10 it was applied an asymmetric distortional mode imperfection and in Figure 12, a local mode imperfection. The local mode initial imperfection leads to a symmetric distortional buckling mode (Figs. Figure 14 and Figure 15).
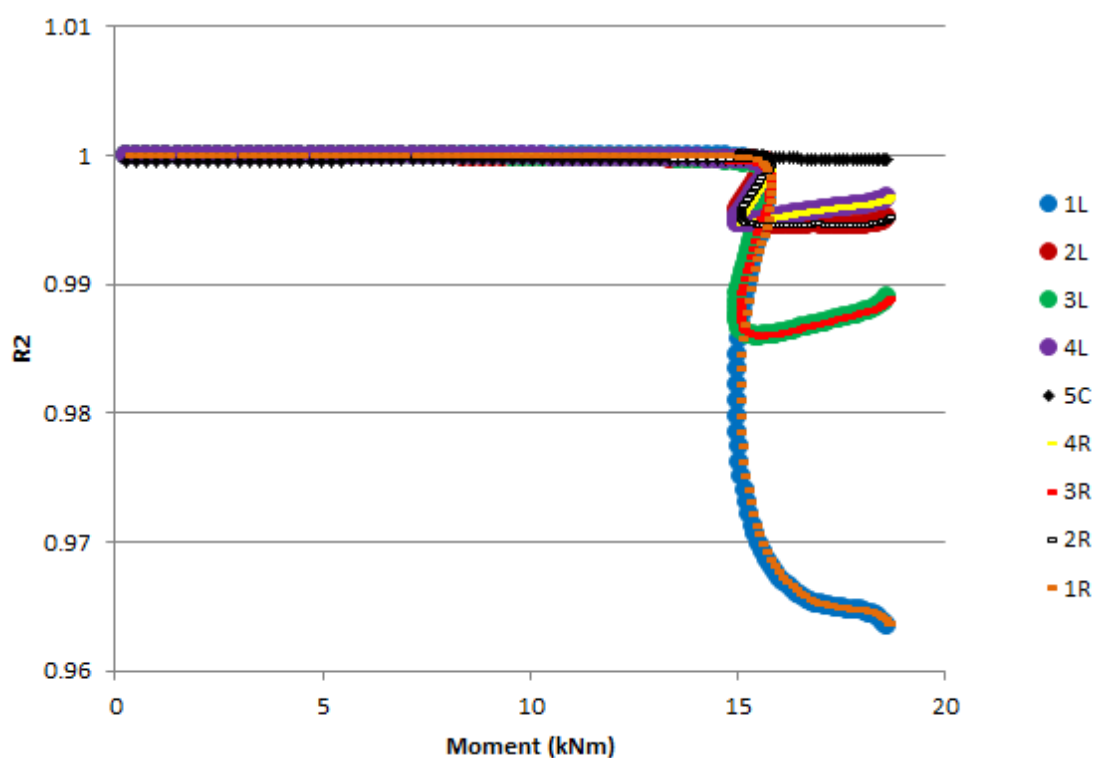
Figure 12: R2 x Moment, trapezoidal stiffener height of 30 mm, local initial imperfection.
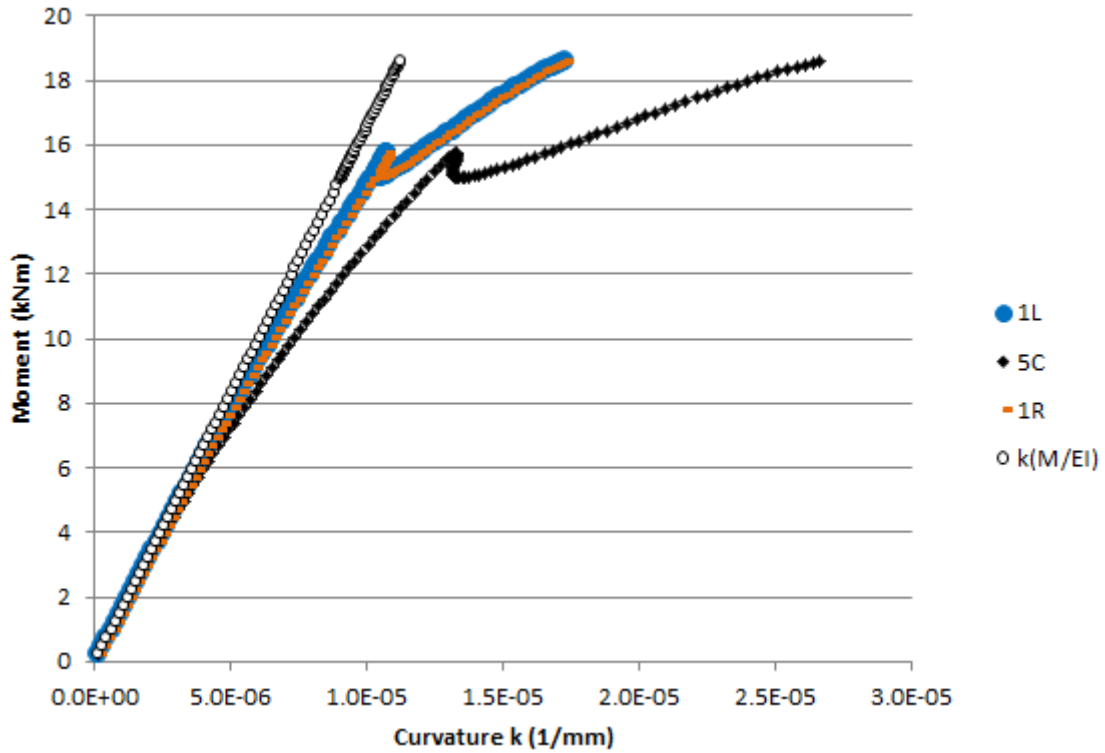
Figure 13: Moment x curvature, trapezoidal stiffener height of 30 mm, local initial imperfection.
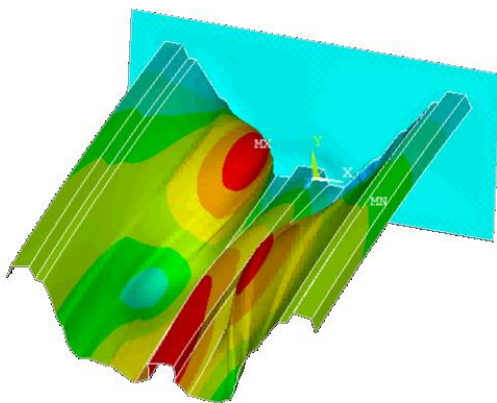
Figure 14: Asymmetric distortional initial imperfection, asymmetric distortional buckling mode.
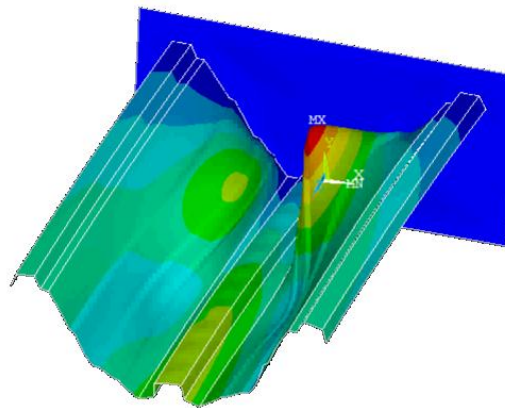
Figure 15: Local imperfection, symmetric distortional buckling mode.

4.2 The R_{LD} ratio and the LD interaction

The Local-Distortional (LD) mode interaction can be measured by the R_{LD} ratio, given by

$$R_{LD} = \frac{M_{crL}}{M_{crD}}$$

where M_{crL} and M_{crD} are the local and distortional critical moments, respectively. The closer the R_{LD} value is to 1, the greater the interaction.

Optimization methods searching for the maximization of critical moments in self-supporting roofing tiles tend to obtain a R_{LD} value close to 1. Varying the height of the trapezoidal stiffener of the RT-260/620 roofing tile, the R_{LD} ratio changes. For a stiffener height of 17 mm in a 0.95 mm thickness tile, it gets closer to 1 (Figure 4).

The R^2 analysis for this LD interaction is shown in Figure 16. When the bending load reaches 15 kNm, the beam buckles in an asymmetric distortional mode. At 16 kNm, a local buckling mode takes place together with the distortional mode. The local buckling can be clearly seen by the drop in the R^2 value of point 5C. Figures Figure 17, Figure 18 and Figure 19 show this sequence of events.
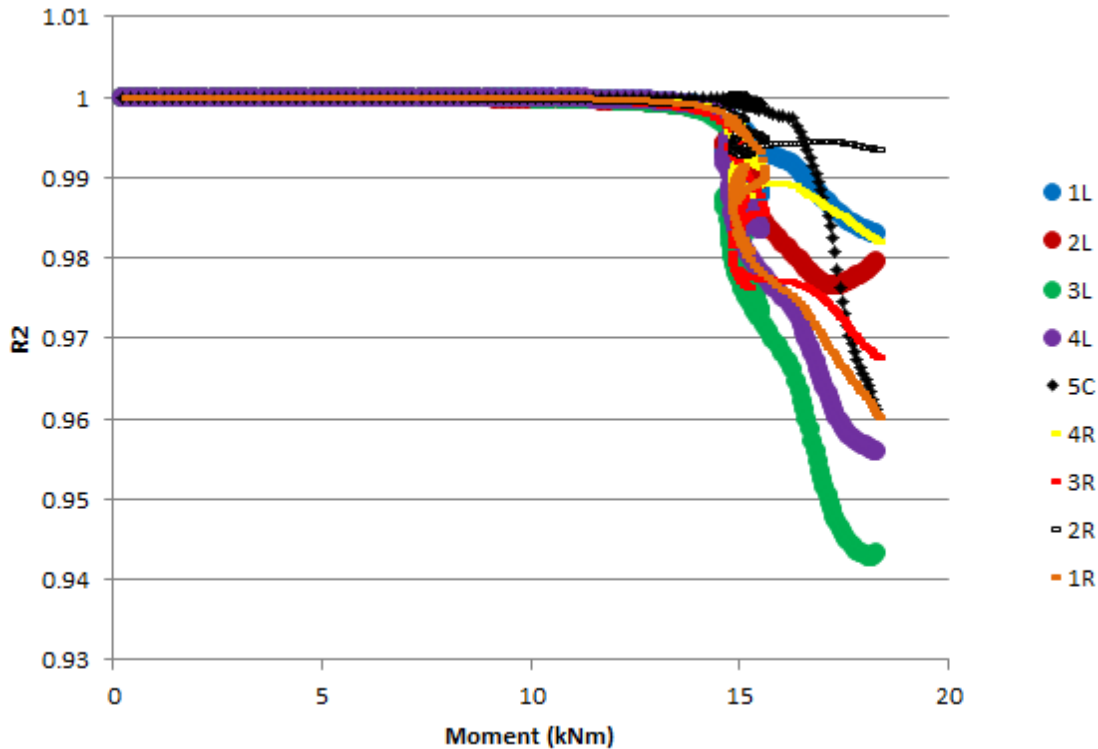
Figure 16: R2 x Moment, trapezoidal stiffener height of 17 mm, distortional initial imperfection.
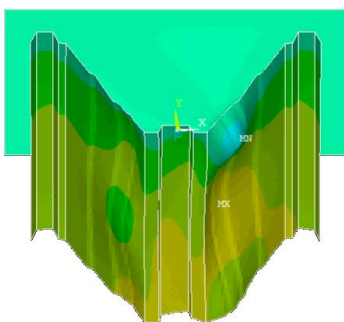
Figure 17: Beginning of the distortional mode (M = 15 kNm).
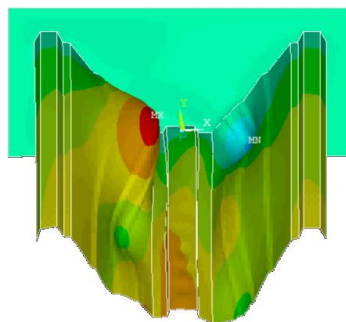
Figure 18: Beginning of the local mode (M = 16 kNm).
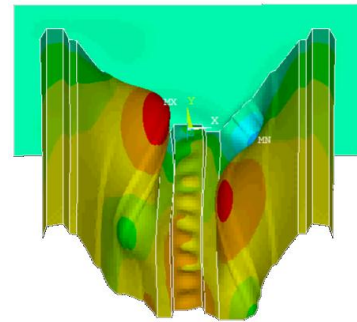
Figure 19: LD mode interaction (M = 18 kNm).

Figure 20 presents the Moment vs. Curvature graph for the trapezoidal stiffener height of 17 mm and a distortional initial imperfection. At 15 kNm, the beam buckles in an asymmetric distortional mode, seen by the difference in curvature for points 1L and 1R, buckling increases the curvature for point 1R, while for point 1L, it reduces slightly. At 16 kNm, a local buckling reduces curvature for points 1R and 5C, and increases curvature for point 1L.
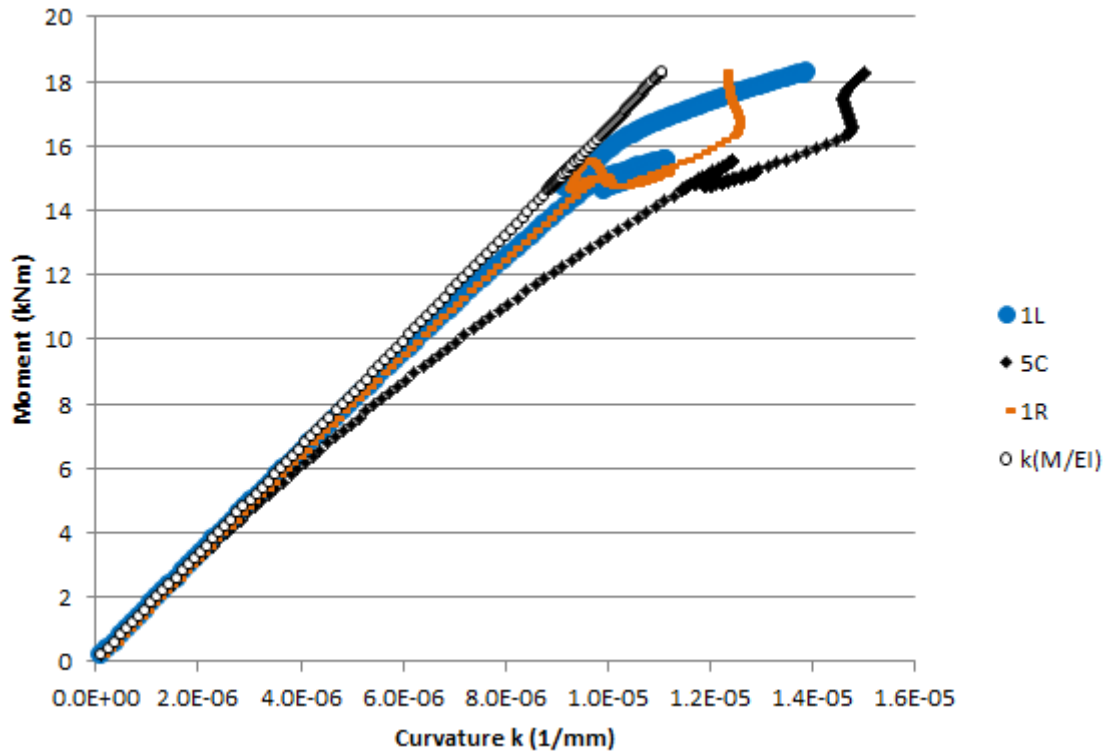
Figure 20: Moment x curvature, trapezoidal stiffener height of 17 mm, distortional initial imperfection.

For the same analysis, but applying a local initial imperfection (Figure 21 and Figure 22), the sequence of events changes (Figs. Figure 23, Figure 24 and Figure 25). At a 12 kNm critical moment, a local buckling mode starts. At 16 kNm, a symmetric distortional buckling mode appears. This symmetric distortional mode makes the bottom flange to dislocate towards the bending elastic line of the beam, in a way to increase the R^2 value, closer to 1, closer to the elastic line (Figure 21).
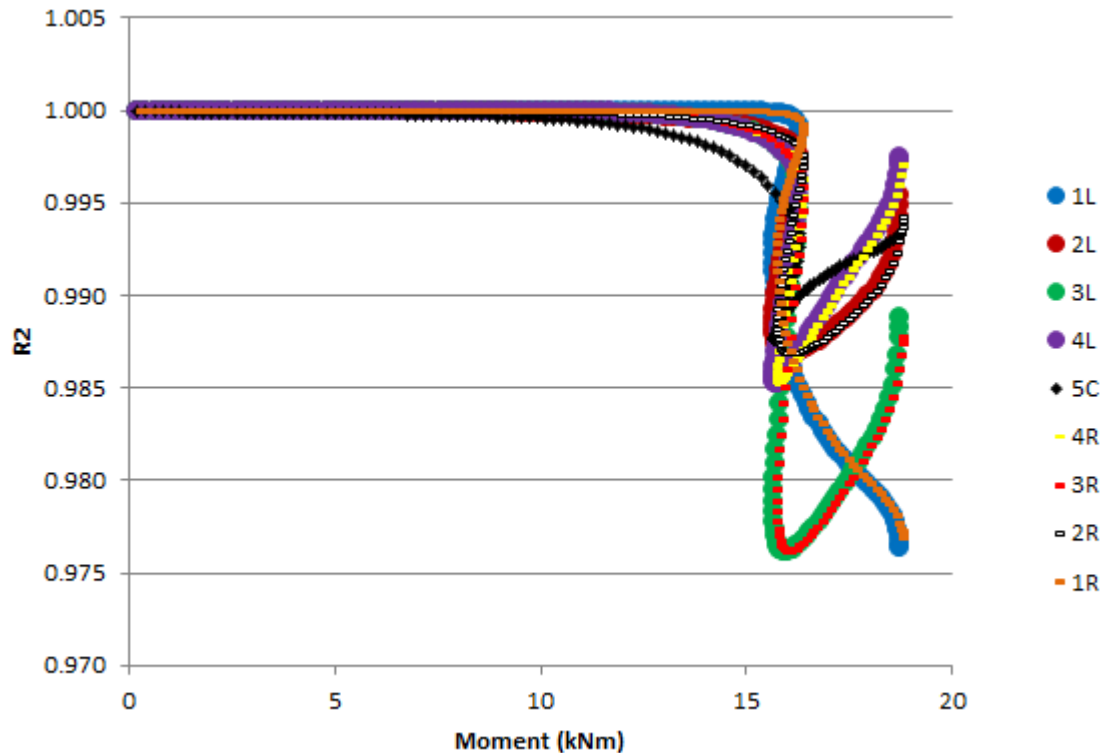
Figure 21: R2 x Moment, trapezoidal stiffener height of 17 mm, local initial imperfection.
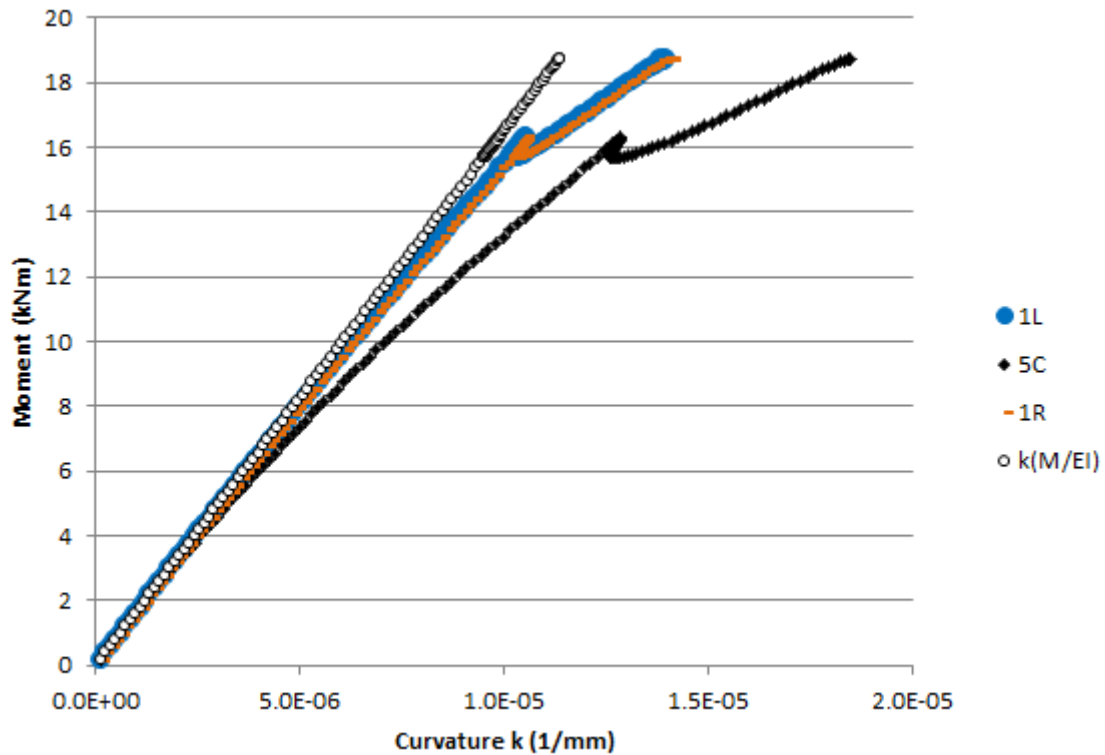
Figure 22: Moment x curvature, trapezoidal stiffener height of 17 mm, local initial imperfection.
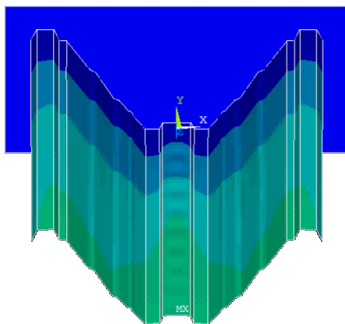
Figure 23: Beginning of the local mode (M = 12 kNm).
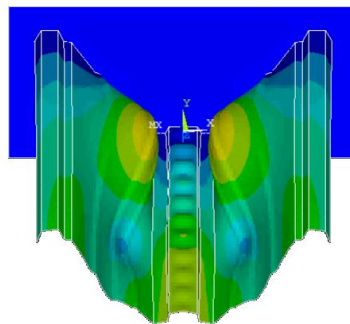
Figure 24: Beginning of the distortional mode (M = 16 kNm).
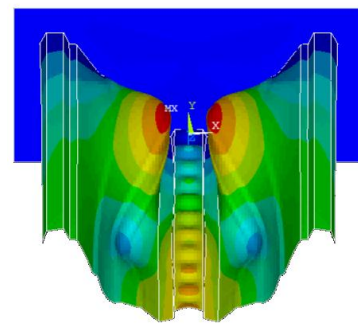
Figure 25: LD mode interaction (M = 19 kNm).

5 Flange curling

A moment vs. curvature graph (Figure 26) from different points along the flanges of the cross-section depicts the flange curling phenomenon. The closer the point is to the web (point 3), the closer the curvature of the point is to the curvature due to bending of the beam (k = M/EI). For the RT-260/620 in bottom compression, the flange curling of the bottom flange (points 3, 4 and 5) increases the curvature of the beam, and the flange curling of the top flange (point 1) decreases the curvature.
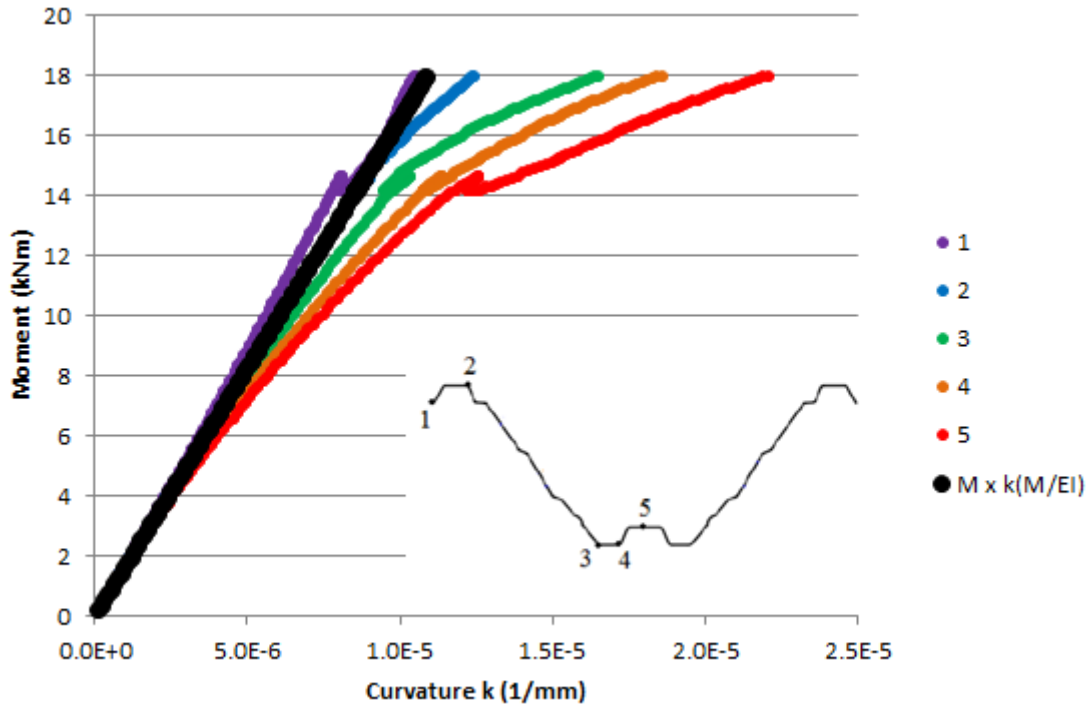
Figure 26: Flange curling in Moment vs. Curvature graph.

6   Final remarks

The results presented for the R^2 coefficient analysis showed up as a good alternative to identify the mode configuration in which the beam buckles after a nonlinear post-buckling analysis. The Finite Strip Method (CUFSM) and the Finite Element model (ANSYS) results for critical moments and buckling mode shapes were in concordance in elastic analysis. However, when performing a nonlinear analysis, the finite element results present different buckling modes, depending on the initial imperfections adopted on the model, showing the sensitiveness of these sections to initial imperfections and the need to take them into account when studying these profiles.

As the bending and flange curling displacements occur before buckling, they can be considered "imperfections" that can affect buckling. Therefore, separating these displacements provide an important way to analyze the beam mechanical behavior, isolating the influence of each of these displacements on the buckling modes and strength of these elements.

Self-supporting roofing steel tiles present a great number of variables (thickness, width, height and slope of the webs and flanges; number, type, size and position of intermediate stiffeners; span length; initial imperfections) and show a considerable sensitiveness to any small change in these variables. This work presents some tools to use in a further parametric modeling in order to evaluate the contribution of each small geometric variation on the critical bending moments and strength.

Acknowledgements

References

[1] Z. LI and B. SCHAFER, "Buckling analysis of cold-formed steel members with general boundary conditions using CUFSM: conventional and constrained finite strip methods," in *Proceedings of the Twentieth International Specialty Conference on Cold-Formed Steel Structures*, Saint Louis, Missouri, USA, 2010.

[2] R. BEBIANO, D. CAMOTIM and R. GONÇALVES, "GBTUL 2.0 – a second-generation code for the GBT-based buckling and vibration analysis of thin-walled members," *Thin-Walled Structures,* vol. 124, pp. 235-253, 2018.

[3] P. DINIS, E. BATISTA, D. CAMOTIM and E. SANTOS, "Local-distortional-global interaction in lipped channel columns: experimental results, numerical simulations and design considerations," *Thin-Walled Structures,* vol. 61, pp. 2-13, 2012.

[4] P. DINIS and D. CAMOTIM, "Cold-formed steel columns undergoing local-distortional coupling: behaviour and direct strength prediction against interactive failure," *Comput. Struct.,* vol. 147, pp. 181-208, 2015.

[5] G. MATSUBARA, E. BATISTA and G. SALLES, "Lipped channel cold-formed steel columns under local-distortional buckling mode interaction," *Thin-Walled Structures,* vol. 137, pp. 251-270, 2019.

[6] E. S. BERNARD, R. Q. BRIDGE and G. J. HANCOCK, "Tests of Profiled Steel Decks with V-Stiffeners," *Journal of Structural Engineering,* vol. 119, no. 8, pp. 2277-2293, 1993.

[7] E. S. BERNARD, R. Q. BRIDGE and G. J. HANCOCK, "Tests of Profiled Steel Decks with Flat-Hat Stiffeners," *J. Struct. Eng.,* vol. 121, no. 8, pp. 1175-1182, 1995.

[8] E. S. BERNARD, R. Q. BRIDGE and G. J. HANCOCK, "Design Methods for Profiled Steel Decks with Intermediate Stiffeners," *J. Construct. Steel Res.,* vol. 38, no. 1, pp. 61-88, 1996.

[9] E. BERNARD and R. BRIDGE, "Flange Curling in Profiled Steel Decks," *Thin-Walled Structures,* vol. 25, no. 1, pp. 1-29, 1996.

[10] G. WINTER, "Stress distribution in and equivalent width of flanges of wide, thin-walled steel beams," NACA technical note 784, Washington DC, 1940.

[11] J. FRANCO, J. DUARTE, E. BATISTA and A. LANDESMANN, "Shape grammar of steel cold-formed sections based on manufacturing rules," *Thin-Walled Struct.,* vol. 79, pp. 218-232, 2014.

[12] J. MELO, J. FRANCO and E. BATISTA, "Sistema generativo e flambagem de seções trapezoidais enrijecidas: aplicação em sistema ortotrópico de cobertura em aço," in *Proceedings in 7o Congresso Latinoamericano da Construção Metálica (Construmetal 2016)*, São Paulo, SP, Brazil, 2016.

[13] J. M. S. FRANCO and E. M. BATISTA, "Buckling behavior and strength of thin-walled stiffened trapezoidal CFS under flexural bending," *Thin-Walled Structures,* pp. 268-281, 2017.

[14] J. P. M. GARCIA, E. M. BATISTA and J. M. S. FRANCO, "Stability and resistance of structural cold-formed steel elements with stiffened sections," in *Ibero-Latin American Congress on Computational Methods in Engineering*, Florianopolis, SC, Brazil, 2017.